Theory of acoustic band structure of periodic elastic composites

M. Kushwaha, P. Halevi, G. Martínez, L. Dobrzynski, B. Djafari-Rouhani

Theory of acoustic band structure of periodic elastic composites

M. S. Kushwaha,* P. Halevi, and G. Martínez
Instituto de Física, Universidad Autónoma de Puebla, Apartado Postal J-48, Puebla 72570, Mexico

L. Dobrzynski and B. Djafari-Rouhani
Laboratoire de Dynamique et Structure de Materiaux Moleculaires, Centre National de la Recherche Scientifique, Universite de Lille I, U.F.R. de Physique-Bâtiment P5, 59655 Villeneuve D'Ascq Cedex, France

(Received 24 August 1993)

We study an elastic composite described by the position-dependent mass density $\rho(\mathbf{r})$, the longitudinal speed of sound $c_l(\mathbf{r})$, and the transverse speed of sound $c_t(\mathbf{r})$. For a spatially periodic composite—a "phononic crystal"—we derive the eigenvalue equation for the frequencies $\omega_n(\mathbf{K})$, where n is the serial number of the band and $\mathbf{K}$ is the Bloch wave vector. This is applied to the special case of a binary composite and, further, to the case of infinite cylinders that form a two-dimensional lattice. For this configuration (and no wave-vector component parallel to the cylinders) there are two independent modes of vibration. The elastic displacement $\mathbf{u}(\mathbf{r})$ is parallel to the cylinders for one of them—the transverse polarization mode. The other one is a mixed (longitudinal-transverse) polarization mode with $\mathbf{u}(\mathbf{r})$ perpendicular to the cylinders. Specifically we consider circular cylinders that form a square lattice. We compute the band structures for the transverse modes of nickel alloy cylinders in an aluminum alloy host, and vice versa. In both situations we find band gaps which extend throughout the Brillouin zone. Within these gaps the transverse vibrations, sound, and phonons are forbidden. We also investigate the dependence of the band gap on the filling fraction and on the material parameters.

I. INTRODUCTION

The last decade has seen a tremendous research interest in the physical properties of artificial structures comprised of two or more materials which differ in certain properties. The 1980s began with enthusiasm for microstructures of reduced dimensionality,[1] such as quantum heterostructures, quantum wires, and quantum dots. More recently there has been ever increasing interest in macrostructures known as "photonic crystals."[2] Typically, these are periodic arrays of two transparent dielectrics. The periodicity plays a crucial role in understanding the physical properties of both microstructures and macrostructures.

In this paper we are concerned with periodic structures that are composed of two or more *elastic* freely vibrating materials. We shall present a detailed theory of acoustic band structure for such composites. Of special interest is the prospect of achieving a complete band gap; this is defined to be a stop band in which vibrations, sound, and phonons are prohibited for all values of the quasi-wave-vector (or Bloch vector) and for both longitudinal and transverse vibrations.

Our inspiration has been drawn from analogous investigations of photonic crystals. These have been studied intensively for the past six years. Due to considerable similarities between the properties of periodic elastic composites and periodic dielectrics, first we shall give a survey of the essential developments related to the latter—photonic crystals.

The initial proposal[3,4] that periodic structures of dielectric materials can be designed to have photonic gaps in which optical modes are forbidden has attracted wide attention, both theoretically[5–18] and experimentally.[19–23] There are many important motivations for pursuing such studies. The absence of electromagnetic (EM) modes inside the photonic gap can lead to unusual physical phenomena.[4,9] For instance, atoms or molecules embedded in a periodic dielectric composite can be locked in an excited state if the energy of this state (relative to the ground state) falls within the forbidden photonic gap.[5] They are also expected to exhibit an anomalous Lamb shift.[9] It has been suggested[3] that inhibition of spontaneous emission in such gaps can be utilized to enhance substantially the performance of semiconductor lasers and other quantum electronic devices. Moreover, John[4] has raised the possibility that the experimental observation of Anderson localization of light could be facilitated by weak disordering of the perfect periodicity of a photonic crystal.

At the outset, theoretical efforts[6–9] devoted to calculating photonic band structures were based on the scalar-wave approximation, much as is done for electron waves in solving the Schrödinger equation. Apart from the fact that scalar-wave theory did not agree well with the experiment,[19] these papers were criticized on the obvious ground of ignoring the vectorial nature of the EM fields. Finally, by employing the full vector Maxwell's equations,[11–13] theorists began to agree with each other as well as with the experiment,[19] except at the high-symmetry points U and W of an fcc crystal. This discrepancy owes to the finite size of the crystal in the experiment.[2]

The experimentally observed pseudogap—rather than a full gap—in the fcc crystal thus triggered concern and a search for a way to overcome the contradiction between theory and experiment. This resulted in a note published in Ref. 24 questioning the existence of a photonic gap in

0163-1829/94/49(4)/2313(10)/$06.00

the band structure of fcc crystals. The outstanding problem was to lift a degeneracy of the bands, particularly at the W point. It was found[13] that if the symmetry of the structure was lowered by filling the Wigner-Seitz unit cell by two atoms, rather than by one, just as in the diamond structure, then a full photonic band gap opened up. This was a significant step taken by Ho, Chan, and Soukoulis[13] since the diamond structure gives a wide photonic band gap for a given dielectric-constant contrast. The quest for crystalline structures that have full photonic band gaps led the same group[25] to propose some periodic arrangements which are related to the diamond structure but are easier to fabricate. One of these, the so-called "three-cylinder structure," was shown to have full photonic gaps in the microwave region.[26]

It was suggested that localization of classical waves (light and sound) could be fostered by some interplay of disorder and (periodic) order.[4,17] According to this argument the study of photonic bands is useful for the elucidation of the conditions that can lead to localization. Since the pioneering work of Anderson[27] and Mott,[28] considerable research efforts have been devoted to the observation of electronic localization in disordered solids. However, successful tests of the scaling theory of localization[29] have been hampered by the nearly inescapable presence of electron-electron interactions and electron-phonon scattering in real materials. Such interactions are nearly absent in classical-wave systems, which is the main reason for the intensive study of elastic-wave and light-wave localization over the past few years.[30–35] For the general aspects of scattering and localization of classical waves in random media, the reader is referred to Ref. 36. Most recently, direct observation of localized elastic waves—the bending waves of a steel plate decorated with lucite blocks—has been reported.[37] These observations are supported by theoretical calculations based on a newly developed "finite-element" method.[18] This methodology is advantageous in applications that call for a description in terms of a complex wave vector.

In a subsequent theoretical development Meade *et al.*[38] examined the effect of terminating the crystal. They computed the EM modes localized at an interface between the air and a photonic crystal half-space. They employed a supercell method in which slabs of dielectric material alternate with slabs of vacuum. It was shown that these surface Bloch waves are localized due to interference effects in the photonic crystal. These surface modes must always exist at the surface of a photonic crystal. Understanding of the surface band structure is of particular importance to the design of lasers[39] which employ vacancies within a photonic crystal.

The proposal of Yablonovitch[3] that a periodic dielectric structure possessing a photonic band gap could lead to inhibited spontaneous emission draws on the early ideas of Kleppner[40] to modify the quantum electrodynamic (QED) vacuum experienced by an atom. The suggestion was[40] that the spontaneous emission by Rydberg atoms and Penning-trapped electrons is inhibited in a small metallic cavity which has no EM modes at the transition frequency. Such a capability is no less important in condensed matter, where spontaneous emission in the form of electron-hole radiative recombination plays a decisive role in limiting the performance of semiconductor lasers, heterojunction bipolar transistors, and solar cells. Recently, Yablonovitch, Gmitter, and Bhat[41] have studied the spontaneous emission of light in thin GaAs double heterostructures. Their observation was that the spontaneous emission rate can be markedly increased or decreased depending on whether the refractive index of the surrounding medium is higher or lower than that of GaAs. Subsequently the inhibition—rather than prohibition—of spontaneous emission has been observed in periodic as well as disordered dielectric structures.[42]

Following the marked success achieved in obtaining photonic band gaps in three-dimensional periodic dielectrics, the interest of theorists[43–46] and experimentalists[22,23] also turned to two-dimensional periodic structures. It is clear that these are relatively easy to fabricate. In these systems one has a periodic array of infinitely long dielectric rods embedded in a different dielectric background. The intersections of the rods with a perpendicular plane form a two-dimensional lattice. The EM waves are assumed to propagate in the plane perpendicular to the rods, and hence decouple into two distinct polarizations. These are the **H** polarization and the **E** polarization corresponding, respectively, to the magnetic and electric fields parallel to the cylinders. Full photonic band gaps were obtained for each polarization with circular cylinders in a square lattice[43] and in a hexagonal lattice.[44,45] It was found that rods with circular cross sections require a lower dielectric-constant contrast to generate a band gap than rods with a square cross section, but do not necessarily yield wider gaps at higher contrasts.[46]

In contrast to the numerous studies of photonic band structures of three- and two-dimensional periodic dielectric structures (photonic crystals), to our knowledge there have been only two elaborate investigations of band structure for "phononic" crystals, namely periodic elastic composites made up of two materials with different elastic properties. In two recent papers[47,48] full acoustic band structures (ABS) for periodic elastic composites have been presented. In both studies a periodic array of parallel rods of circular cross sections was embedded in a different background. The intersections of these rods with a perpendicular plane form a square lattice. Kushwaha *et al.*[48] considered only the transverse polarization mode—with displacement $\mathbf{u}(\mathbf{r},t)$ parallel to the cylinders (and perpendicular to the Bloch wave vectors). The numerical computation was performed for Ni (Al) cylinders in an Al (Ni) background. Absolute acoustic or phononic band gaps, extending throughout the first Brillouin zone, were found in the low-frequency regimes in both cases. Sigalas and Economou[47] also studied the mixed, longitudinal-transverse, polarization mode for which $\mathbf{u}(\mathbf{r},t)$ (as well as the Bloch vectors) is perpendicular to the cylinders' axis. They found that gold cylinders in Be exhibit a narrow, however complete gap, shared by both polarizations.

In analogy to the photonic crystals, in the frequency range of a phononic band gap, vibrations, sound, and phonons are forbidden. Thus a vibrator or a small (real)

crystal introduced into a periodic composite as a defect would be unable to generate sound or phonons within the band gap. From a practical point of view, a complete acoustic band gap could be engineered to provide a vibrationless environment for high-precision mechanical systems in a given frequency range. Piezoelectric and pyroelectric periodic composites have had long-standing applications as transducers for transmitting and receiving signals in water.[49] These are used in sonar and depth-finding systems (at frequencies of tens of KHz and above),[50] and have also been designed for medical ultrasonic imaging (0.5–20 MHz).[51] It should be pointed out that corresponding computations of acoustic band structure were very limited in scope.[52,53] Understanding the full band structure of elastic composites could lead to improvements in the design of transducers. Finally, we expect that carefully fabricated, periodic elastic composites with moderate disorder may have important consequences for the localization of vibrational and sound waves.

In this paper we present a detailed theory of the band structure of periodic elastic composites, assuming that only isotropic materials are involved. Equivalent theoretical calculations were performed in Refs. 52–54. However, the band-structure computations in Refs. 52 and 53 were limited to a single direction in the Brillouin zone and were not concerned with the question of a complete acoustic band gap. As for Ref. 54, the authors' interest lay in the low-frequency limit, in which they calculated the elastic moduli for periodic composites.

In Sec. II we start by deriving the general equation of motion for an inhomogeneous medium that supports coupled (longitudinal and transverse) modes. In Sec. III we present the derivation of a general secular equation used to calculate the acoustic band structure of an elastic composite of arbitrary periodicity. It is noteworthy that nowhere have we made use of boundary conditions. Section IV is devoted to the special case of binary composites, namely the unit cell is composed of only two materials. In Sec. V, we restrict ourselves to two-dimensional periodicity by assuming a translational symmetry along one direction which is perpendicular to the plane of wave propagation. Numerical results for the acoustic band structure of the two-dimensional square lattice are given for a specific (transverse) polarization in Sec. VI.

II. WAVE EQUATION FOR AN INHOMOGENEOUS ELASTIC MEDIUM

We consider an inhomogeneous, however isotropic elastic solid of infinite extension. At every point $\mathbf{r}$ the medium is characterized by three material parameters: the mass density $\rho(\mathbf{r})$, the longitudinal speed of sound $c_l(\mathbf{r})$, and the transverse speed of sound $c_t(\mathbf{r})$. In terms of these the stress tensor assumes the form

$$\sigma_{iK}=2\rho c_t^2 u_{iK}+\rho(c_l^2-2c_t^2)u_{ll}\delta_{iK} , \tag{1}$$

where

$$u_{iK}=\frac{1}{2}\left[\frac{\partial u_i}{\partial x_K}+\frac{\partial u_K}{\partial x_i}+\frac{\partial u_l}{\partial x_i}\frac{\partial u_l}{\partial x_K}\right] \tag{2}$$

is the deformation tensor, u_i ($i=1,2,3$) being the components of the displacement vector $\mathbf{u}(\mathbf{r},t)$. The convention of summation over equal indices applies.

In the absence of external forces Newton's Second Law takes the form

$$\rho\frac{\partial^2 u_i}{\partial t^2}=\frac{\partial \sigma_{iK}}{\partial x_K} \tag{3}$$

$$=2\rho c_t^2\frac{\partial u_{iK}}{\partial x_K}+\rho(c_l^2-2c_t^2)\frac{\partial u_{ll}}{\partial x_K}\delta_{iK}+2u_{iK}\frac{\partial}{\partial x_K}(\rho c_t^2)+u_{ll}\delta_{iK}\frac{\partial}{\partial x_K}(\rho c_l^2-2\rho c_t^2) . \tag{4}$$

Now we shall restrict the treatment to linear media, thereby omitting the quadratic term in u_i in Eq. (2). Then Eq. (4) simplifies to

$$\rho\frac{\partial^2 u_i}{\partial t^2}=\rho c_t^2\nabla^2 u_i+\rho(c_l^2-c_t^2)\frac{\partial}{\partial x_i}\nabla\cdot\mathbf{u}+\nabla(\rho c_t^2)\cdot\nabla u_i+\nabla(\rho c_t^2)\cdot\frac{\partial\mathbf{u}}{\partial x_i}+\left[\frac{\partial}{\partial x_i}(\rho c_l^2-2\rho c_t^2)\right]\nabla\cdot\mathbf{u} . \tag{5}$$

After some algebra this can be brought to the form

$$\rho\frac{\partial^2 u_i}{\partial t^2}=\nabla\cdot(\rho c_t^2\nabla u_i)+\nabla\cdot\left[\rho c_t^2\frac{\partial\mathbf{u}}{\partial x_i}\right]+\frac{\partial}{\partial x_i}[(\rho c_l^2-2\rho c_t^2)\nabla\cdot\mathbf{u}] . \tag{6}$$

This compact form of the law of motion is particularly convenient because it allows us to avoid applying messy boundary conditions, as we shall see. Of course Eq. (6) is the wave equation for an inhomogeneous elastic medium. It is complicated because, with ρ, c_t, and c_l being position dependent, this equation *cannot* be separated into two equations, one for the longitudinal displacement (that satisfies $\nabla\times\mathbf{u}=\mathbf{0}$), and the other for the transverse displacement (with $\nabla\cdot\mathbf{u}=0$).

III. BAND-STRUCTURE CALCULATION FOR PERIODIC INHOMOGENEITY

The wave equation (6) is valid for arbitrary inhomogeneity. Now we focus attention on an inhomogeneous medium which exhibits spatial periodicity. This implies that the material constants $\rho(\mathbf{r})$, $c_l(\mathbf{r})$, and $c_t(\mathbf{r})$ may all be expanded in the Fourier series. Actually it is convenient to expand ρc_l^2 and ρc_t^2, rather than c_l and c_t themselves:

$$\rho(\mathbf{r})=\sum_{\mathbf{G}}\rho(\mathbf{G})e^{i\mathbf{G}\cdot\mathbf{r}} , \tag{7a}$$

$$\rho(\mathbf{r})c_l^2(\mathbf{r})=\sum_{\mathbf{G}}\Lambda(\mathbf{G})e^{i\mathbf{G}\cdot\mathbf{r}} , \tag{7b}$$

$$\rho(\mathbf{r})c_t^2(\mathbf{r})=\sum_{\mathbf{G}}\tau(\mathbf{G})e^{i\mathbf{G}\cdot\mathbf{r}} . \tag{7c}$$

The periodicity of the medium may be three, two, or one dimensional, and the reciprocal-lattice vector $\mathbf{G}$ has corresponding dimensionality. The summation in Eq. (7) extends over the infinite reciprocal lattice that corresponds to the Bravais lattice in real space. The displacement $\mathbf{u}(\mathbf{r})$ must satisfy the Bloch theorem

$$\mathbf{u}(\mathbf{r},t)=e^{i(\mathbf{K}\cdot\mathbf{r}-\omega t)}\sum_{\mathbf{G}}\mathbf{u}_{\mathbf{K}}(\mathbf{G})e^{i\mathbf{G}\cdot\mathbf{r}}\ , \tag{8}$$

where $\mathbf{K}$ is the Bloch wave vector, and ω is the circular frequency of the wave. Equations (7) and (8) must be substituted into Eq. (6). Straightforward vector algebra, then multiplication by $\exp(-i\mathbf{G}''\cdot\mathbf{r})$, and integration over the unit cell gives the result—for convenience in vector form—

$$\begin{aligned}\sum_{\mathbf{G}'}\{&\tau(\mathbf{G}-\mathbf{G}')\mathbf{u}_{\mathbf{K}}(\mathbf{G}')(\mathbf{K}+\mathbf{G}')\cdot(\mathbf{K}+\mathbf{G})\\&+\tau(\mathbf{G}-\mathbf{G}')\mathbf{u}_{\mathbf{K}}(\mathbf{G}')\cdot(\mathbf{K}+\mathbf{G})(\mathbf{K}+\mathbf{G}')\\&+[\Lambda(\mathbf{G}-\mathbf{G}')-2\tau(\mathbf{G}-\mathbf{G}')]\mathbf{u}_{\mathbf{K}}(\mathbf{G}')\cdot(\mathbf{K}+\mathbf{G}')(\mathbf{K}+\mathbf{G})\\&-\omega^2\rho(\mathbf{G}-\mathbf{G}')\mathbf{u}_{\mathbf{K}}(\mathbf{G}')\}=0\ .\end{aligned} \tag{9}$$

If we allow $\mathbf{G}$ to take all the points of the reciprocal lattice, then Eq. (9) is an infinite set of linear equations for the eigenvectors $\mathbf{u}_{\mathbf{K}}(\mathbf{G})$. For a given value of the Bloch vector $\mathbf{K}$ this set of equations has solutions for some eigenvalues $\omega_n(\mathbf{K})$, where $n=1,2,\ldots$ is the first, second, etc. vibrational band. Notice that, in the derivation, no recourse was made to boundary conditions.

One may inquire whether Eq. (9) simplifies if the polarization dependence is taken into account explicitly, separating $\mathbf{u}_{\mathbf{K}}(\mathbf{G})$ into a longitudinal part (parallel to $\mathbf{K}+\mathbf{G}$), and into two transverse parts (perpendicular to $\mathbf{K}+\mathbf{G}$). Unfortunately this is not the case.

IV. BINARY COMPOSITE

In this case every unit cell is composed of only two materials, labeled a and b. Thus material a (b) is characterized by the parameters ρ_a (ρ_b), c_{la} (c_{lb}), and c_{ta} (c_{tb}). In addition we must specify the occupancy ratios, which are f and $(1-f)$ for the materials a and b. The Fourier coefficients in Eqs. (7) now take a particularly simple form. First consider $\rho(\mathbf{G})$, given by

$$\rho(\mathbf{G})=V_c^{-1}\int d^3r\,\rho(\mathbf{r})e^{-i\mathbf{G}\cdot\mathbf{r}}\ , \tag{10}$$

where the integration is over the unit cell and V_c is its volume. For two-dimensional periodicity d^3r is replaced by d^2r, and V_c is replaced by the area of the unit cell A_c. For $\mathbf{G}=\mathbf{0}$, Eq. (10) gives simply the average density, hence

$$\rho(\mathbf{G}=\mathbf{0})=\bar{\rho}=\rho_a f+\rho_b(1-f)\ .$$

If $\mathbf{G}\neq\mathbf{0}$ we can write

$$\rho(\mathbf{G})=V_c^{-1}\rho_a\int_a d^3r\,e^{-i\mathbf{G}\cdot\mathbf{r}}+V_c^{-1}\rho_b\int_b d^3r\,e^{-i\mathbf{G}\cdot\mathbf{r}}\ .$$

The first (second) integration covers only material a (b). This may be also written as

$$\begin{aligned}\rho(\mathbf{G})=&V_c^{-1}\rho_b\int_{a+b}d^3r\,e^{-i\mathbf{G}\cdot\mathbf{r}}\\&+V_c^{-1}(\rho_a-\rho_b)\int_a d^3r\,e^{-i\mathbf{G}\cdot\mathbf{r}}\ .\end{aligned}$$

The integral in the first term is identically zero. The integral in the second term defines a structure function

$$F(\mathbf{G})=V_c^{-1}\int_a d^3r\,e^{-i\mathbf{G}\cdot\mathbf{r}}\ . \tag{11}$$

Then we have

$$\rho(\mathbf{G})=\begin{cases}\rho_a f+\rho_b(1-f)\equiv\bar{\rho}, & \mathbf{G}=\mathbf{0}\\(\rho_a-\rho_b)F(\mathbf{G})\equiv(\Delta\rho)F(\mathbf{G}), & \mathbf{G}\neq\mathbf{0}\ .\end{cases} \tag{12}$$

In an entirely similar way Eqs. (7b) and (7c) give

$$\Lambda(\mathbf{G})=\begin{cases}\rho_a c_{la}^2 f+\rho_b c_{lb}^2(1-f)\equiv\overline{\rho c_l^2}\equiv\bar{\Lambda}, & \mathbf{G}=\mathbf{0}\\(\rho_a c_{la}^2-\rho_b c_{lb}^2)F(\mathbf{G})\equiv\Delta(\rho c_l^2)F(\mathbf{G})\equiv(\Delta\Lambda)F(\mathbf{G}), & \mathbf{G}\neq\mathbf{0}\ ,\end{cases} \tag{13}$$

$$\tau(\mathbf{G})=\begin{cases}\rho_a c_{ta}^2 f+\rho_b c_{tb}^2(1-f)\equiv\overline{\rho c_t^2}\equiv\bar{\tau}, & \mathbf{G}=\mathbf{0}\\(\rho_a c_{ta}^2-\rho_b c_{tb}^2)F(\mathbf{G})\equiv\Delta(\rho c_t^2)F(\mathbf{G})\equiv(\Delta\tau)F(\mathbf{G}), & \mathbf{G}\neq\mathbf{0}\ .\end{cases} \tag{14}$$

The structure function $F(\mathbf{G})$, Eq. (11), is of course the same in Eqs. (12)–(14). The results are still valid in the two-dimensional case, with the aforementioned replacements in Eq. (11). Also notice that in evaluating $F(\mathbf{G})$ the vector $\mathbf{G}$ is arbitrary, which is to say that the *form* of the structure factor $F(\mathbf{G})$ does not depend on the type of the Bravais lattice, but only on the geometry of the "atom" a.

If in Eq. (9) we single out the term $\mathbf{G}'=\mathbf{G}$ in the summation, then this equation may be rewritten as

$$\begin{aligned}&(\bar{\tau}|\mathbf{K}+\mathbf{G}|^2-\bar{\rho}\omega^2)\mathbf{u}_{\mathbf{K}}(\mathbf{G})+(\bar{\Lambda}-\bar{\tau})(\mathbf{K}+\mathbf{G})(\mathbf{K}+\mathbf{G})\cdot\mathbf{u}_{\mathbf{K}}(\mathbf{G})\\&+\sum_{\mathbf{G}'\neq\mathbf{G}}F(\mathbf{G}-\mathbf{G}')\{(\Delta\tau)[(\mathbf{K}+\mathbf{G})\cdot(\mathbf{K}+\mathbf{G}')\mathbf{u}_{\mathbf{K}}(\mathbf{G}')+(\mathbf{K}+\mathbf{G}')(\mathbf{K}+\mathbf{G})\cdot\mathbf{u}_{\mathbf{K}}(\mathbf{G}')-2(\mathbf{K}+\mathbf{G})(\mathbf{K}+\mathbf{G}')\cdot\mathbf{u}_{\mathbf{K}}(\mathbf{G}')]\\&+(\Delta\Lambda)(\mathbf{K}+\mathbf{G})(\mathbf{K}+\mathbf{G}')\cdot\mathbf{u}_{\mathbf{K}}(\mathbf{G}')-(\Delta\rho)\omega^2\mathbf{u}_{\mathbf{K}}(\mathbf{G}')\}=0\ .\end{aligned} \tag{15}$$

In general there is no simplification of this formidable equation. It can be expressed in dyadic notation, with $\overleftrightarrow{I}$ denoting the unit dyad:

$$[(\bar{\tau}|\mathbf{K}+\mathbf{G}|^2-\bar{\rho}\omega^2)\overleftrightarrow{I}+(\bar{\Lambda}-\bar{\tau})(\mathbf{K}+\mathbf{G})(\mathbf{K}+\mathbf{G})]\cdot\mathbf{u}_{\mathbf{K}}(\mathbf{G})+\sum_{\mathbf{G}'\neq\mathbf{G}}F(\mathbf{G}-\mathbf{G}')\overleftrightarrow{U}(\mathbf{G},\mathbf{G}')\cdot\mathbf{u}_{\mathbf{K}}(\mathbf{G}')=0\ , \tag{16a}$$

$$\overleftrightarrow{U}(\mathbf{G},\mathbf{G}')=(\Delta\tau)[(\mathbf{K}+\mathbf{G})\cdot(\mathbf{K}+\mathbf{G}')\overleftrightarrow{I}+(\mathbf{K}+\mathbf{G}')(\mathbf{K}+\mathbf{G})-2(\mathbf{K}+\mathbf{G})(\mathbf{K}-\mathbf{G}')]+(\Delta\Lambda)(\mathbf{K}+\mathbf{G})(\mathbf{K}+\mathbf{G}')-(\Delta\rho)\omega^2\overleftrightarrow{I}\ . \tag{16b}$$

We see that, for a binary composite, the material parameters may be grouped into "average parameters" $\bar{\rho}$, $\bar{\Lambda}$, and $\bar{\tau}$ and "contrast parameters" $\Delta\rho$, $\Delta\Lambda$, and $\Delta\tau$. In practice the band structure is rendered in terms of dimensionless quantities. While we derive Eq. (15) for arbitrary crystalline symmetry and arbitrary composition of the unit cell, it is convenient to introduce some lattice parameter a for the sake of normalization. We define the following quantities:

$$\mathbf{k}=\mathbf{K}a/2\pi,\quad \mathbf{g}=\mathbf{G}a/2\pi\ , \tag{17}$$

$$\Omega=\omega a/2\pi C_t\ , \tag{18}$$

$$C_t=(\bar{\tau}/\bar{\rho})^{1/2}=(\overline{\rho c_t^2}/\bar{\rho})^{1/2}\ , \tag{19}$$

$$C_l=(\bar{\Lambda}/\bar{\rho})^{1/2}=(\overline{\rho c_l^2}/\bar{\rho})^{1/2}\ , \tag{20}$$

$$\gamma=\left[\frac{\bar{\Lambda}}{\bar{\tau}}\right]^{1/2}=\left[\frac{f\rho_a c_{la}^2/\rho_b c_{lb}^2+1-f}{f\rho_a c_{ta}^2/\rho_b c_{tb}^2+1-f}\right]^{1/2}\frac{c_{lb}}{c_{tb}}\ , \tag{21}$$

$$\delta\rho=\frac{\Delta\rho}{\bar{\rho}}=\frac{\rho_a/\rho_b-1}{f\rho_a/\rho_b+1-f}\ , \tag{22}$$

$$\delta\Lambda=\frac{\Delta\Lambda}{\bar{\Lambda}}=\frac{\rho_a c_{la}^2/\rho_b c_{lb}^2-1}{f\rho_a c_{la}^2/\rho_b c_{lb}^2+1-f}\ , \tag{23}$$

$$\delta\tau=\frac{\Delta\tau}{\bar{\tau}}=\frac{\rho_a c_{ta}^2/\rho_b c_{tb}^2-1}{f\rho_a c_{ta}^2/\rho_b c_{tb}^2+1-f}\ . \tag{24}$$

Now Eq. (15) takes the form

$$\begin{aligned}&(|\mathbf{k}+\mathbf{g}|^2-\Omega^2)\mathbf{u}_{\mathbf{k}}(\mathbf{g})+(\gamma^2-1)(\mathbf{k}+\mathbf{g})(\mathbf{k}+\mathbf{g})\cdot\mathbf{u}_{\mathbf{k}}(\mathbf{g})\\&\quad+\sum_{\mathbf{g}'\neq\mathbf{g}}F(\mathbf{g}-\mathbf{g}')\{(\delta\tau)[(\mathbf{k}+\mathbf{g})\cdot(\mathbf{k}+\mathbf{g}')\mathbf{u}_{\mathbf{k}}(\mathbf{g}')+(\mathbf{k}+\mathbf{g}')(\mathbf{k}+\mathbf{g})\cdot\mathbf{u}_{\mathbf{k}}(\mathbf{g}')-2(\mathbf{k}+\mathbf{g})(\mathbf{k}+\mathbf{g}')\cdot\mathbf{u}_{\mathbf{k}}(\mathbf{g}')]\\&\qquad+\gamma^2(\delta\Lambda)(\mathbf{k}+\mathbf{g})(\mathbf{k}+\mathbf{g}')\cdot\mathbf{u}_{\mathbf{k}}(\mathbf{g}')-(\delta\rho)\Omega^2\mathbf{u}_{\mathbf{k}}(\mathbf{g}')\}=0\ .\end{aligned} \tag{25}$$

From the last equation it is apparent that it is convenient to plot the dimensionless frequency Ω versus the dimensionless wave vector $\mathbf{k}$. Then one must supply the four dimensionless parameters γ, $\delta\rho$, $\delta\Lambda$, and $\delta\tau$. From Eqs. (21)–(24) we see that the input involves the ratios ρ_a/ρ_b, C_{la}/C_{lb}, C_{ta}/C_{tb}, and C_{lb}/C_{tb}, as well as the occupancy f. The last term in the curly brackets of Eq. (25) is proportional to Ω^2, which means that the matrix operating on $\mathbf{u}_{\mathbf{k}}$ depends on the eigenvalue. A very substantial saving in computational time is achieved by transforming Eq. (25) into the form

$$\sum_{\mathbf{g}'}\overleftrightarrow{A}_{\mathbf{g}\mathbf{g}'}(\mathbf{k})\cdot\mathbf{u}_{\mathbf{k}}(\mathbf{g})=\Omega^2\mathbf{u}_{\mathbf{k}}(\mathbf{g})\ , \tag{26}$$

with the "dyadic matrix" $\overleftrightarrow{A}$ independent of Ω. The existence of such a matrix implies that its elements must be computed only for every value of $\mathbf{k}$, rather than for every value of $\mathbf{k}$ *and* Ω. We note, however, that Eq. (26) does *not* have the form of the *standard* eigenvalue problem. This is because the left side of this equation couples the three components of $\mathbf{u}_{\mathbf{k}}$. The difficulty stems from the inseparability, in general, of the longitudinal and transverse modes of vibration.

In order to derive the expression for $\overleftrightarrow{A}_{\mathbf{g}\mathbf{g}'}(\mathbf{k})$, we express Eq. (25) in the form

$$\sum_{\mathbf{g}'}\overleftrightarrow{M}_{\mathbf{g}\mathbf{g}'}\cdot\mathbf{u}_{\mathbf{k}}(\mathbf{g}')=\Omega^2\sum_{\mathbf{g}'}N_{\mathbf{g}\mathbf{g}'}\,\mathbf{u}_{\mathbf{k}}(\mathbf{g})\ , \tag{27a}$$

$$\begin{aligned}\overleftrightarrow{M}_{\mathbf{g}\mathbf{g}'}&=|\mathbf{k}+\mathbf{g}|^2\overleftrightarrow{I}\delta_{\mathbf{g}\mathbf{g}'}+(\gamma^2-1)(\mathbf{k}+\mathbf{g})(\mathbf{k}+\mathbf{g})\delta_{\mathbf{g}\mathbf{g}'}\\&\quad+F(\mathbf{g}-\mathbf{g}')\{(\delta\tau)[(\mathbf{k}+\mathbf{g})\cdot(\mathbf{k}+\mathbf{g}')\overleftrightarrow{I}+(\mathbf{k}+\mathbf{g}')(\mathbf{k}+\mathbf{g})-2(\mathbf{k}+\mathbf{g})(\mathbf{k}+\mathbf{g}')]+\gamma^2(\delta\Lambda)(\mathbf{k}+\mathbf{g})(\mathbf{k}+\mathbf{g}')\}(1-\delta_{\mathbf{g}\mathbf{g}'})\ ,\end{aligned} \tag{27b}$$

$$N_{\mathbf{g}\mathbf{g}'}=\delta_{\mathbf{g}\mathbf{g}'}+F(\mathbf{g}-\mathbf{g}')(\delta\rho)(1-\delta_{\mathbf{g}\mathbf{g}'})\ , \tag{27c}$$

where $\delta_{gg'}$ is the Kronecker delta. Equation (27a) may be rewritten in matrix form as

$$\vec{\mathbf{M}}\cdot\mathbf{u}_{\mathbf{k}}=\Omega^2 N\mathbf{u}_{\mathbf{k}} . \tag{28}$$

If we operate on this equation, from the left, by the inverse of the matrix N, namely N^{-1}, we have

$$N^{-1}\vec{\mathbf{M}}\cdot\mathbf{u}_{\mathbf{k}}=\Omega^2\mathbf{u}_{\mathbf{k}} . \tag{29}$$

Therefore the matrix $\vec{\mathbf{A}}$ defined in Eq. (26) is given by

$$\vec{\mathbf{A}}=N^{-1}\vec{\mathbf{M}} . \tag{30}$$

This expression is independent of Ω, for which benefit we pay the relatively small price of having to invert the matrix N and having to perform the multiplication $N^{-1}\vec{\mathbf{M}}$.

Once the crystalline symmetry and the structure of the unit cell have been specified, Eq. (26) with the definitions (30) and (27b) and (27c), is the starting point for the calculation of the bands $\Omega_n(\mathbf{k})$.

V. TWO-DIMENSIONAL PERIODICITY

First we only assume that the system has translational symmetry in one direction (z). This means that the material parameters $\rho(\mathbf{r})$, $C_l(\mathbf{r})$, and $C_t(\mathbf{r})$ in this case depend only on the coordinates x and y. We also limit the wave propagation to the xy plane—an assumption which follows all the studies, both theoretical and experimental, on the photonic band structure of dielectric cylinders. Then the displacement $\mathbf{u}$ is also independent of the z coordinate. Here we use the notation (x,y,z) for the coordinates, rather than (x_1,x_2,x_3) as in Sec. II.

Taking the x component of Eq. (6), we have now

$$\rho\frac{\partial^2 u_x}{\partial t^2}=\nabla_T\cdot(\rho c_t^2\nabla_T u_x)+\nabla_T\cdot\left[\rho c_t^2\frac{\partial\mathbf{u}_T}{\partial x}\right]+\frac{\partial}{\partial x}[(\rho c_l^2-2\rho c_t^2)\nabla_T\cdot\mathbf{u}_T] , \tag{31}$$

where $\mathbf{u}_T=\hat{x}u_x+\hat{y}u_y$ and $\nabla_T=\hat{x}(\partial/\partial x)+\hat{y}(\partial/\partial y)$. The y component of Eq. (6) is obtained by the replacement $x\rightarrow y$. For the z component, we get

$$\rho\frac{\partial^2 u_z}{\partial t^2}=\nabla_T\cdot(\rho c_t^2\nabla_T u_z) . \tag{32}$$

From Eqs. (31) and (32) there follows the important conclusion that the vibrations of this system fall into two distinct categories: vibrations in the transverse plane ($\mathbf{u}_T$) and vibrations parallel to the translational axis ($\hat{z}u_z$); these variations are independent of each other and are governed by Eqs. (31) and (32), respectively. In Eq. (31) the longitudinal and transverse sound velocities both appear, hence the longitudinal and transverse vibrations remain coupled. We shall call this mode the "mixed polarization mode." On the other hand, in Eq. (32) only c_t appears, as one can expect from the fact that the vibration $\hat{z}u_z$ is perpendicular to the plane xy in which the wave propagation takes place. This then is a "transverse polarization mode."

We see that Eq. (32), which governs the behavior of the transverse polarization mode, is considerably simpler than Eq. (31). In fact, in Ref. 1 our starting point was Eq. (32), and there we considered only the transverse mode.

Now let us restrict attention to a binary composite with periodicity in the xy plane. This is to say that we have a periodic array of identical, infinite cylinders of an arbitrary cross section. Rather than pursuing Eqs. (31) and (32) we shall proceed from our general result for a periodic binary system, Eq. (15). Now $\mathbf{G}$ is the two-dimensional reciprocal-lattice vector in the xy plane. Because we have restricted wave propagation to the same plane, the Bloch vector $\mathbf{K}$ is also two dimensional. If we take the component perpendicular to z of Eq. (15), an examination of this equation reveals that the only change is the replacement $\mathbf{u}(\mathbf{G})\rightarrow\mathbf{u}_T(\mathbf{G})=\hat{x}u_x(\mathbf{G})+\hat{y}u_y(\mathbf{G})$, where the index $\mathbf{K}$ has been suppressed. For the z component we find

$$[\bar{\tau}|\mathbf{K}+\mathbf{G}|^2-\bar{\rho}\omega^2]u_{\mathbf{K}}(\mathbf{G})+\sum_{\mathbf{G}'\neq\mathbf{G}}[(\Delta\tau)(\mathbf{K}+\mathbf{G})\cdot(\mathbf{K}+\mathbf{G}')-(\Delta\rho)\omega^2]\times F(\mathbf{G}-\mathbf{G}')u_{\mathbf{K}}(\mathbf{G}')=0 . \tag{33}$$

Here $u_{\mathbf{K}}(\mathbf{G})$ denotes the z component of $\mathbf{u}_{\mathbf{K}}(\mathbf{G})$, the index z having been omitted.

Equation (15), with $\mathbf{u}$ replaced by $\mathbf{u}_T$, can also be obtained from Eq. (31), and it leads to the band structure for the mixed-polarization mode. Equation (33) also follows from Eq. (32); it is the starting point for the band-structure calculation of the transverse mode, and it was the final result in Ref. 1. The mixed mode will be the subject of a subsequent study, and from this point on we shall consider only the transverse mode.

It is useful to rewrite Eq. (33) in terms of the quantities defined in Eqs. (17), (18), (22), and (24). The formula also follows from Eq. (25),

$$(|\mathbf{k}+\mathbf{g}|^2-\Omega^2)u_{\mathbf{k}}(\mathbf{g})+\sum_{\mathbf{g}'\neq\mathbf{g}}F(g-g')[(\delta\tau)(\mathbf{k}+\mathbf{g})\cdot(\mathbf{k}+\mathbf{g}')-(\delta\rho)\Omega^2]\times u_{\mathbf{k}}(\mathbf{g}')=0 . \tag{34}$$

It is apparent that if we plot Ω against k then the only parameters that ought to be specified are $\delta\rho$, $\delta\tau$, and f. By Eqs. (22) and (24) this is equivalent to giving ρ_a/ρ_b, C_{ta}/C_{tb}, and f. Clearly, in this particular configuration, the computation and interpretation of results are bound to be much less involved. The procedure outlined between Eqs. (26) and (30) now simplifies. The matrix elements $N_{\mathbf{g}'}$ are still given by Eq. (27c); however, in Eq.

(27b) for $\overleftrightarrow{M}_{gg'}$ we can omit all the terms that terminate with $(\mathbf{k}+\mathbf{g})$ and $(\mathbf{k}+\mathbf{g}')$. This is because the scalar products of these factors with $\mathbf{u}_\mathbf{k}$ in Eq. (28) vanish for the transverse mode. This leaves us with the terms in $\overleftrightarrow{M}_{gg'}$ that are proportional to $\overleftrightarrow{I}$. Because $\overleftrightarrow{I}\cdot\mathbf{u}_\mathbf{k}=\mathbf{u}_\mathbf{k}=U_\mathbf{k}\hat{z}$, it is convenient to replace $\overleftrightarrow{M}_{gg'}$ by the scalar matrix

$$M_{gg'}=|\mathbf{k}+\mathbf{g}|^2\delta_{gg'} + F(\mathbf{g}-\mathbf{g}')(\delta\tau)(\mathbf{k}+\mathbf{g})\cdot(\mathbf{k}+\mathbf{g}')(1-\delta_{gg'}) . \quad (35)$$

Then the matrix A in Eq. (30) also becomes scalar, and Eq. (26) is replaced by

$$\sum_{g'} A_{gg'}(\mathbf{k})U_\mathbf{k}(\mathbf{g}')=\Omega^2 U_\mathbf{k}(\mathbf{g}) . \quad (36)$$

This equation, unlike Eq. (26), corresponds to the *standard* eigenvalue form.

In order to evaluate the structure factor $F(\mathbf{G})$ we must specify the cross-sectional form of the cylinders a. This we choose to be a circle. Then, with the origin coinciding with the center of the circle, Eq. (11) gives

$$F(\mathbf{G})=A_c^{-1}\int_0^{r_0} r\,dr\int_0^{2\pi} e^{-iGr\cos\theta}d\theta ,$$

where r_0 is the radius of the cylinder. The result is

$$F(\mathbf{G})=A_c^{-1}2\pi r_0 J_1(Gr_0)/G ,$$

J_1 being the Bessel function of the first kind of order 1. The filling fraction is

$$f=\pi r_0^2/A_c , \quad (37)$$

so this can be rewritten as

$$F(\mathbf{G})=2fJ_1(Gr_0)/(Gr_0) . \quad (38)$$

The last step is to specify the symmetry of the lattice. The only specific Bravais lattice to be considered in this paper is the square lattice. Its reciprocal lattice is also square, with the reciprocal-lattice vectors given by

$$\mathbf{G}=(2\pi/a)(n_x\hat{x}+n_y\hat{y}) , \quad (39)$$

where a is the lattice constant and n_x and n_y assume all the integer values. The corresponding dimensionless vector is $\mathbf{g}=n_x\hat{x}+n_y\hat{y}$. The argument of the Bessel function in Eq. (38) can be written as

$$Gr_0=[4\pi f(n_x^2+n_y^2)]^{1/2} . \quad (40)$$

With the substitutions (38)–(40) in Eq. (34), once the parameters $\delta\rho$ (or ρ_a/ρ_b), $\delta\tau$ (or c_{ta}/c_{tb}), and f have been given, we are ready for the computation of eigenvalues $\Omega(\mathbf{k})$ and eigenvectors $u_\mathbf{K}(\mathbf{g})$.

VI. NUMERICAL RESULTS FOR THE SQUARE LATTICE

As has been pointed out earlier, we confine our attention to binary elastic composites with two-dimensional periodicity. The crystal is an array of cylinders of circular cross section, whose intersections with a perpendicular plane form a square lattice. This means that our structure factor $F(\mathbf{G})$ is specified by Eq. (38) and the secular equation used to compute the band structure is Eq. (36) which corresponds to the standard eigenvalue problem. The integers n_x and n_y were permitted to take the values in the interval defined by $-10\le n_x, n_y\le+10$ (441 plane waves). This resulted in very good convergence. The relevant material parameters are $\rho=8.936$ (2.697) gm/cm^3 and $C_{44}(=\rho c_t^2)=7.54$ (2.79) $\times10^{11}$ dyn/cm^2 for Ni (Al) alloy.[55]

Figure 1 shows the first ten bands for Ni alloy cylinders in an Al alloy background. The figure is comprised of three parts. In the first part, we have plotted the band structure in the three principal symmetry directions, letting $\mathbf{k}$ scan the periphery of the irreducible

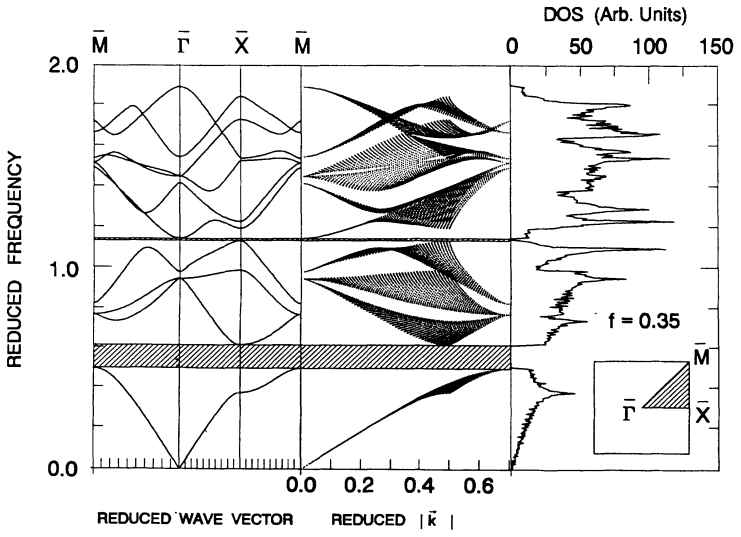

FIG. 1. Acoustic band structure and density of states for Ni alloy cylinders in an Al alloy matrix. The figure is comprised of three parts. In the first part, we plot the band structure in the three principal symmetry directions letting $\mathbf{k}$ scan the periphery of the triangle $\bar{\Gamma}\bar{X}\bar{M}$. The second part of this figure illustrates the eigenvalues Ω_n as a function of $|\mathbf{k}|$; i.e., the distance of a point in the irreducible part of the Brillouin zone from the $\bar{\Gamma}$ point. The third part shows the density of states. The material parameters are $\rho=8.936$ (2.697) gm/cm^3, $C_{44}(=\rho c_t^2)=7.54$ (2.79)$\times10^{11}$ dyn/cm^2 for Ni (Al) alloy, and $f=0.35$. Attention is drawn to the photonic band gap between the first two bands extending throughout the first Brillouin zone.

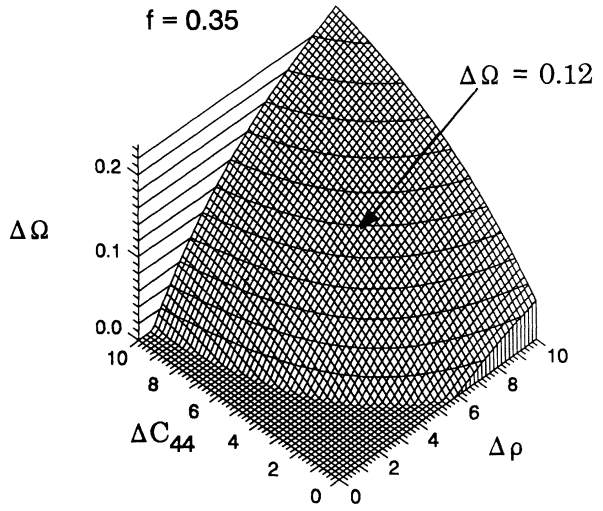

FIG. 2. Magnitude of the lowest band gap as a function of the differences (contrasts) in the elastic constant and in the density. We emphasize that this three-dimensional plot provides a guide to the feasibility of designing phononic band gaps by an appropriate choice of the materials for a binary composite. Here $f=0.35$, just as in Fig. 1. The contrast parameters have the same units as defined in Fig. 1.

triangle of the first Brillouin zone. We obtain a phononic band gap opened by between the first two bands. For this value of the filling fraction ($f=0.35$), there is another, very narrow band gap lying between the fourth and the fifth bands, with $\Delta\Omega\simeq 0.02$. (There are no higher gaps, at least as far as the 50th band.) The second part of this figure illustrates an interesting way to present the band structure; namely, now we plot the eigenvalues Ω_n as a function of $|\mathbf{k}|$, i.e., the distance of a point in the Brillouin zone from the origin. We have scanned not only the periphery but also the interior of the irreducible triangle $\bar{\Gamma}\,\bar{X}\,\bar{M}$ of the Brillouin zone (see the inset of Fig. 1). This part of the computation embodies 1326 values in the uniformly distributed grid of $\mathbf{k}$ points throughout the irreducible part of the Brillouin zone. Using the same number of $\mathbf{k}$ points, we have computed the density of states (DOS), plotted in the third part of the figure. The magnitudes of the phononic gaps coincide in the second and third parts of the figure, which leads us to infer that the existing band gaps extend throughout the Brillouin zone. This in turn establishes the fact that wave propagation in the transverse plane is forbidden for vibrations parallel to the cylinders. The value of the normalized gap width in this case is $\Delta\Omega\simeq 0.12$.

We now examine the magnitude of the lowest band gap as a function of variations in the elastic constant and density. The geometry is the same as for Fig. 1, that is Ni alloy cylinders in an Al alloy matrix. The numerical results, for $f=0.35$, are depicted in Fig. 2. Note that ΔC_{44} and $\Delta\rho$ stand for

$$\Delta C_{44}=C_{44}^{a}-C_{44}^{b}=\rho_a c_{ta}^2-\rho_b c_{tb}^2,\quad \Delta\rho=\rho_a-\rho_b\ .$$

The superscripts a and b refer to the cylinder and the background, respectively. This three-dimensional plot contains a wealth of information about the existence of phononic band gaps and the choice of the materials to create such gaps. For instance, the arrow (on the right-hand side of this surface) indicates our explicit choice of the materials producing a gap given by $\Delta\Omega=0.12$ (see Fig. 1). In other words, the plot in Fig. 2 provides a guide to the feasibility of designing the phononic band gaps by an appropriate choice of the materials for a binary composite. In particular, let us comment that according to Fig. 2 large gaps require that the contrasts $\Delta\rho$ and ΔC_{44} both be large. Here we have explored only the case that $\rho_a>\rho_b$ and $C_{44}^{a}>C_{44}^{b}$.

Now we turn to the situation where Al alloy cylinders are embedded in a Ni alloy background. The numerical results are illustrated by the specific example $f=0.75$ in

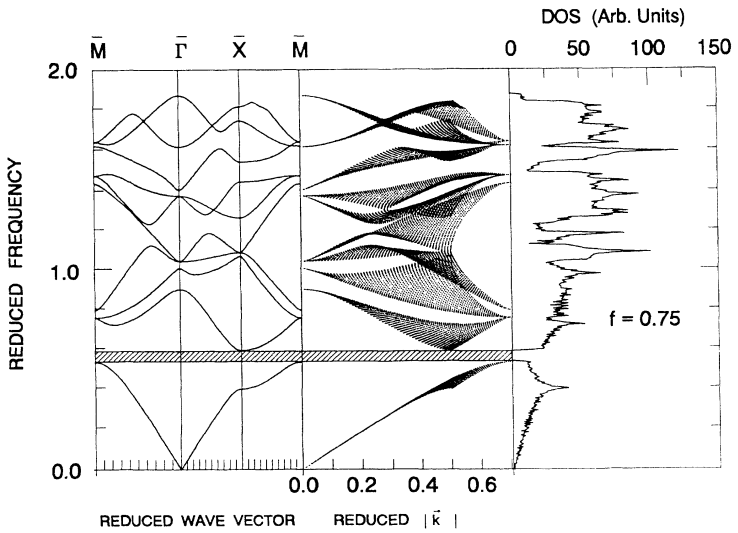

FIG. 3. The same as in Fig. 1, but for Al alloy cylinders in a Ni alloy matrix. The filling fraction is $f=0.75$.

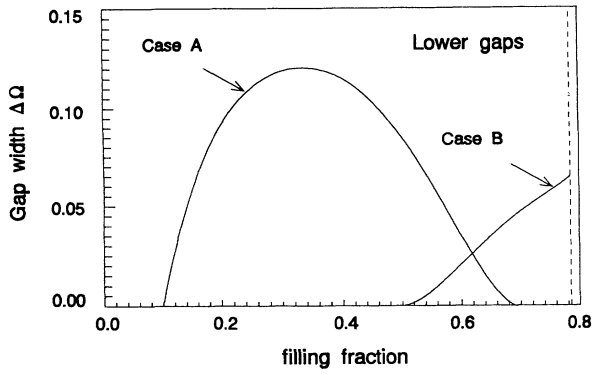

FIG. 4. The width of the lowest band gap as a function of filling fraction. Case A (case B) refers to the Ni (Al) alloy cylinders in Al (Ni) alloy background.

Fig. 3. We find one phononic band gap opened up between the first two bands. The existence and magnitude of this gap is well established by the complete band structure (central part of this figure) and by the density of states (the third part of the figure). It is thus concluded that this phononic gap extends throughout the Brillouin zone. The rest of the discussion related to Fig. 1 is still valid. It is noteworthy that there are no phononic gaps opening up above the second band, or up to the 50th band, at least.

Finally, we examine the width of the lower gap as a function of filling fraction for both cases. The numerical results are shown in Fig. 4. The curve marked case A (case B) represents the situation with Ni (Al) alloy cylinders in the Al (Ni) alloy matrix. It is found that the largest gap in case A corresponds to the filling fraction $f \simeq 0.33$. Similarly, the largest gap in case B opens up at a filling fraction corresponding to the close packing ($f \simeq 0.7854$). It is noteworthy that, in case A, an absolute gap opens up over a large range of filling fraction defined by $0.10 \leq f \leq 0.69$. In case B, on the other hand, there is no phononic gap for $f \leq 0.52$.

ACKNOWLEDGMENT

M.S.K. and P.H. acknowledge CONACyT Grant No. 2048-E9302.

*Present address: Instituto de Ciencia de Materiales, CSIC, Serrano 123, 28006 Madrid, Spain.
[1]L. L. Chang and L. Esaki, Phys. Today **45**, 36 (1992).
[2]E. Yablonovitch, J. Phys. Condens. Matter **5**, 2443 (1993).
[3]E. Yablonovitch, Phys. Rev. Lett. **58**, 2059 (1987).
[4]S. John, Phys. Rev. Lett. **58**, 2486 (1987).
[5]G. Kurizki and A. Z. Genack, Phys. Rev. Lett. **61**, 2269 (1988).
[6]S. John and R. Rangarajan, Phys. Rev. B **38**, 10 101 (1988).
[7]E. N. Economou and A. Zdetsis, Phys. Rev. B **40**, 1334 (1988).
[8]S. Satpathy, Z. Zhang, and M. R. Salehpur, Phys. Rev. Lett. **64**, 1239 (1990).
[9]S. John and J. Wang, Phys. Rev. Lett. **64**, 2418 (1990).
[10]K. M. Leung and Y. F. Liu, Phys. Rev. B **41**, 10 188 (1990).
[11]K. M. Leung and Y. F. Liu, Phys. Rev. Lett. **65**, 2646 (1990).
[12]Z. Zhang and S. Satpathy, Phys. Rev. Lett. **65**, 2650 (1990).
[13]K. M. Ho, C. T. Chan, and C. M. Soukoulis, Phys. Rev. Lett. **65**, 3152 (1990).
[14]R. D. Meade, K. D. Brommer, A. M. Rappe, and J. D. Joannopoulos, Phys. Rev. B **44**, 13 772 (1991).
[15]S. Satpathy and Z. Zhang, Mod. Phys. Lett. **5**, 1041 (1991).
[16]H. S. Sözüer, J. W. Haus, and R. Inguva, Phys. Rev. B **45**, 13 962 (1992).
[17]S. Datta, C. T. Chan, K. M. Ho, and C. M. Soukoulis, Phys. Rev. B **46**, 10 650 (1992).
[18]J. B. Pendry and A. Mackinnon, Phys. Rev. Lett. **69**, 2772 (1992).
[19]E. Yablonovitch and T. J. Gmitter, Phys. Rev. Lett. **63**, 1950 (1989).
[20]E. Yablonovitch, T. J. Gmitter, and K. M. Leung, Phys. Rev. Lett. **67**, 2295 (1991).
[21]E. Yablonovitch, T. J. Gmitter, R. D. Meade, A. M. Rappe, K. D. Brommer, and J. D. Joannopoulos, Phys. Rev. Lett. **67**, 3380 (1991).
[22]S. L. McCall, P. M. Platzman, R. Dalichaouch, D. Smith, and S. Schultz, Phys. Rev. Lett. **67**, 2017 (1991).
[23]W. M. Robertson, G. Arjavalingam, R. D. Meade, K. D. Brommer, A. M. Rappe, and J. D. Joannopoulos, Phys. Rev. Lett. **68**, 2023 (1992).
[24]J. Madox, Nature **348**, 481 (1990).
[25]C. T. Chan, K. M. Ho, and C. M. Soukoulis, Europhys. Lett. **16**, 563 (1991).
[26]E. Yablonovitch and K. M. Leung, Nature **351**, 278 (1991).
[27]P. W. Anderson, Phys. Rev. **109**, 1492 (1958).
[28]N. F. Mott, Adv. Phys. **16**, 49 (1967).
[29]E. Abrahams, P. W. Anderson, D. C. Licciardello, and T. V. Ramakrishnan, Phys. Rev. Lett. **42**, 673 (1979).
[30]S. John, Phys. Rev. Lett. **63**, 2169 (1984).
[31]P. W. Anderson, Philos. Mag. B **52**, 505 (1985).
[32]P. Sheng and Z. Q. Zhang, Phys. Rev. Lett. **57**, 1879 (1986).
[33]S. He and J. D. Maynard, Phys. Rev. Lett. **57**, 3171 (1986).
[34]S. John, Comments Condens. Matter. Phys. **14**, 193 (1988); Phys. Today **44**, 32 (1991).
[35]A. Z. Genack and N. García, Phys. Rev. Lett. **66**, 2064 (1991).
[36]*Scattering and Localization of Classical Waves in Random Media*, edited by P. Sheng (World Scientific, Singapore, 1990).
[37]L. Ye, G. Cody, M. Zhou, P. Sheng, and A. N. Norris, Phys. Rev. Lett. **69**, 3080 (1992).
[38]R. D. Meade, K. D. Brommer, A. M. Rappe, and J. D. Joannopoulos, Phys. Rev. B **44**, 10 961 (1991).
[39]P. L. Gourley, M. E. Warren, G. A. Vawter, T. M. Brennan, and B. E. Hammons, Appl. Phys. Lett. **60**, 2714 (1992); **61**, 1484 (1992).
[40]D. Kleppner, Phys. Rev. Lett. **47**, 233 (1981); R. G. Hulet, E. S. Hilfer, and D. Kleppner, Phys. Rev. Lett. **55**, 2137 (1985).
[41]E. Yablonovitch, T. J. Gmitter, and R. Bhat, Phys. Rev. Lett. **61**, 2546 (1988).
[42]J. Martorell and N. M. Lawandy, Phys. Rev. Lett. **65**, 1877 (1990); **66**, 887 (1991).

[43]M. Plihal, A. Shambrook, A. A. Maradudin, and P. Sheng, Opt. Commun. **80**, 199 (1991).
[44]M. Plihal and A. A. Maradudin, Phys. Rev. B **44**, 8565 (1991).
[45]P. R. Villeneuve and M. Piche, Phys. Rev. B **46**, 4969 (1992).
[46]P. R. Villeneuve and M. Piche, Phys. Rev. B **46**, 4973 (1993).
[47]M. Sigalas and E. N. Economou, Solid State Commun. **86**, 141 (1993). See also E. N. Economou and M. Sigalas, in *Photonic Band Gaps and Localization,* edited by C. M. Soukoulis (Plenum, New York, 1993), p. 317; M. Sigalas and E. N. Economou, J. Sound Vibration **158**, 377 (1992).
[48]M. S. Kushwaha, P. Halevi, L. Dobrzysnki, and B. Djafari-Rouhani, Phys. Rev. Lett. **71**, 2022 (1993).
[49]B. A. Auld, Mater. Sci. Eng. A **122**, 65 (1989).
[50]A. A. Shaulov, W. A. Smith, and B. M. Singer, in *Proceedings of the Ultrasonic Symposium* (IEEE, New York, 1984), p. 539. W. A. Smith, A. A. Shaulov, and B. A. Auld, *ibid.* 1985, p. 642.
[51]W. A. Smith and B. A. Auld, IEEE Trans. Ultrason. Ferroelectrics, Frequency Control **38**, 40 (1991).
[52]B. A. Auld, in *Ultrasonic Methods in Evaluation of Inhomogeneous Materials,* edited by A. Alippi and W. G. Mayer (Nijhoff, Dordrecht, 1987), p. 227; B. A. Auld, Y. A. Shui, and Y. Wang, J. Phys. (Paris) **45**, 159 (1984).
[53]S. Baste and A. Gerard, Ref. 51, p. 381.
[54]Ruibao Tao and Ping Sheng, J. Acous. Soc. Am. **77**, 1651 (1985).
[55]*American Institute of Physics Handbook,* 3rd ed. (AIP, New York, 1972).